Surface Science 646 (2016) 154–159

Contents lists available at ScienceDirect

Surface Science

journal homepage: www.elsevier.com/locate/susc

Surface studies of lithium–oxygen redox reactions over HOPG

Florencia Marchini, Santiago E. Herrera, Ernesto J. Calvo, Federico J. Williams *

Departamento de Química Inorgánica, Analítica y Química Física, INQUIMAE-CONICET, Facultad Ciencias Exactas y Naturales, Universidad de Buenos Aires, Ciudad Universitaria, Pabellón 2, Buenos Aires C1428EHA, Argentina

ARTICLE INFO

Available online 6 August 2015

Keywords:
Lithium–air batteries
XPS
AFM
Oxygen reduction
HOPG
Electrochemistry

ABSTRACT

The O_2/Li_2O_2 electrode reaction has been studied on low surface area HOPG electrodes in 0.1 M $LiPF_6$ in dimethyl sulfoxide (DMSO) electrolyte. Studies were performed using electrochemical cells coupled to a XPS spectrometer and to an AFM microscope. AFM images after electrochemical treatment at cathodic potentials exhibited 20 to 100 nm in height features, whereas anodic treatment showed a thin film of about 1 nm thickness deposited over the HOPG electrode. XPS spectra after electrochemical treatment showed surface species due to DMSO and $LiPF_6$ decomposition. These findings indicate the high reactivity of oxygen reduction products towards the electrolyte and the solvent. The unwanted deposits formed under electrochemical operation cannot be completely eliminated from the surface even after applying high anodic potentials. This highlights the known loss of capacity of Li-air batteries, issue that must be overcome for successful applications.

1. Introduction

The rechargeable lithium–air battery exhibits a very large theoretical energy density with potential electric vehicle applications with extended millage range [1–5]. In the non-aqueous Li–air battery during discharge a Li anode dissolves in the electrolyte and the resulting Li^+ ions react with O_2 reduction products at a porous carbon cathode to form insoluble Li_2O_2 [1–6]. Two parallel mechanisms for the electroreduction of O_2 in lithium electrolytes with strong solvation of Li^+ are now accepted [7,8]: i) a surface superoxide disproportionation or two consecutive electron oxygen reduction reactions (ORR) and ii) a solution phase mechanism with soluble lithium peroxide disproportionation and precipitation forming large toroidal Li_2O_2 particles [9,10]. The prevalence of each mechanism would depend on the current density [9] and the presences of water traces [7]. Two major drawbacks of this advanced lithium–air battery are the high overpotential during recharge and the battery capacity fading. The first problem is associated to the formation of large insulating lithium peroxide particles while the second one is related to the high reactivity of lithium superoxide and peroxide towards the electrolyte and the solvent. Therefore, fundamental understanding of the ORR and lithium peroxide oxidation reactions in non-aqueous electrolytes is necessary to develop lithium–air batteries technology.

Among non-aqueous solvents, dimethyl sulfoxide (DMSO) with a very large dipolar moment ($\mu = 4{,}3$ D) has been used in re-chargeable batteries with 95% capacity retention in 100 cycles [11–14]. However, there is a controversy on the stability of insoluble Li_2O_2 produced since the balance of O_2 consumed in the ORR and that evolved in the oxygen evolution reaction (OER) during charging is always less than 0.9 [15]. While the ORR is a 2-electron process yielding Li_2O_2, the outermost surface of Li_2O_2 may react chemically with the electrolyte and/or the solvent decomposing them and decreasing the amount of peroxide on the surface [16,17]. Differential electrochemical mass spectrometry (DEMS) with different solvent–electrolyte pairs has shown that the moles of O_2 measured upon charge are significantly below the number expected for complete peroxide formation and decomposition in agreement with the loss of capacity observed during cycling [4,15,18–20].

In parallel, there has been recent evidence of DMSO decomposition mainly to carbonate species when placed in contact with solid Li_2O_2. Other side products such as LiOH, dimethyl sulfone, Li_2SO_3 and Li_2SO_4, have also been detected [21,22]. XPS studies have shown that DMSO decomposes at the Li_2O_2 solid/liquid solvent interface while acetonitrile showed no evidence of degradation [22]. In addition $LiPF_6$, $LiBF_4$ and $LiClO_4$ were reported to react with Li_2O_2 to generate LiF and other species [21–23]. Aurbach has recently confirmed the instability of DMSO for Li–air batteries with electrochemical quartz crystal microbalance (EQCM) measurements [24]. Recent results with rotating ring-disk electrode and EQCM have shown the stability of lithium superoxide in DMSO electrolyte and the co-deposition of the solvent during the formation of Li_2O_2 deposits on the electrode surface [7,25].

While most studies have been conducted using large surface area electrodes or bulk battery materials, the present investigation explores the composition at the electrode using highly oriented pyrolytic graphite (HOPG) as a model system for carbon electrode material. Photoelectron spectroscopy measurements were carried out after applying selected electrode potentials in O_2 saturated 0.1 M $LiPF_6$ in DMSO using an electrochemical cell coupled to a UHV system to ensure no

* Corresponding author. Tel.: +54 11 45763380x105.
E-mail address: fwilliams@qi.fcen.uba.ar (F.J. Williams).

http://dx.doi.org/10.1016/j.susc.2015.07.028
0039-6028/

ambient contamination of the surfaces. AFM, XPS and UPS experiments after O_2 reduction showed surface species due to DMSO and $LiPF_6$ decomposition that persists even after applying high anodic potentials. This finding gives further evidence regarding the loss of capacity in the cycling of the battery due to undesirable side reactions.

2. Experimental methods

2.1. Materials

Anhydrous dimethyl sulfoxide ≥ 99.9% and lithium hexafluorophosphate battery grade ≥ 99.99% were obtained from SIGMA-ALDRICH and stored in an argon-filled MBRAUN glove box with oxygen content ≤ 0.1 ppm and water content below 2 ppm. DMSO was dried for several days over 3 Å molecular sieves (SIGMA-ALDRICH). All solutions were prepared inside the glove box and water content was measured using a Karl Fisher 831 KF Coulometer (Metrohm). All solutions employed were found to contain initially around 30 ppm of water. Highly oriented pyrolytic graphite (HOPG) substrates were cleaned by removing the topmost layers by mechanical exfoliation with adhesive tape.

2.2. Photoelectron spectroscopy measurements

XPS and UPS measurements were performed using an ultrahigh vacuum chamber (UHV; base pressure $< 5 \times 10^{-10}$ mbar) equipped with a transfer system built in our laboratory that allows easy and rapid controlled transfer of the sample between the UHV environment and the atmospheric (Ar or O_2) liquid electrochemical environment. This transfer system serves the purpose to perform ex-situ electron spectroscopic measurements on samples that are initially clean in UHV and are not exposed to the laboratory atmosphere before or after electrochemical measurements (described in detailed elsewhere [26]). Electrochemical measurements were carried out using a cell with a three-electrode configuration consisting of a platinum counter electrode, a Pt wire coated with a $LiMn_2O_4/Li_2Mn_2O_4$ deposit as the reference electrode and the sample as the working electrode (also described in detailed elsewhere [26]). The reference electrode potential measured in a glove box with respect to a lithium foil in 0.1 M $LiPF_6$/DMSO was 3.25 V and all potentials herein are referred to the Li/Li^+ system in the respective electrolyte. Typical electrochemical experiments involve transferring the HOPG sample from the UHV environment to the electrochemical cell without exposure to the laboratory atmosphere at any moment. The HOPG sample forms a meniscus with an O_2 saturated 0.1 M $LiPF_6$ in DMSO solution in an O_2 atmosphere. Electrochemical cyclic voltammetry or chronoamperometry measurements are performed at room temperature using an operational amplifier potentiostat (TEQ Argentina). Then the HOPG sample is removed from solution at fixed potential, extensively rinsed with pure dry DMSO, dried under a constant flow of Argon and transferred back to the analysis chamber. The analysis chamber is equipped with a SPECS UHV spectrometer system consisting of a 150 mm mean radius hemispherical electron energy analyzer and a nine channeltron detector. XP spectra were acquired on grounded conducting substrates at a constant pass energy of 20 eV using a Mg Kα (1253.6 eV) source operated at 12.5 kV and 20 mA at a detection angle of 30° with respect to the sample normal. Binding energies are referred to the HOPG C 1s emission at 284.7 eV. No charge compensation was necessary and no differential charging features were observed (e.g. low binding energy tails) given that we have measured sufficiently thin films on grounded conducting substrates. Atomic ratios were calculated from the integrated intensities of core levels after instrumental and photoionization cross section corrections. UPS spectra were acquired using a He I radiation source (21.2 eV) operated at 100 mA with normal detection at a constant pass energy of 2 eV.

2.3. Atomic force microscopy

AFM imaging was performed in air using an Agilent 5500 scanning probe microscope (Agilent Technologies) isolated from vibrations, air turbulence and acoustic noise, before and after electrochemical experiments. The three electrode EC-AFM electrochemical cell employed consists of a Pt gauze counter electrode, $LiMn_2O_4/Li_2Mn2O_4$/Pt reference electrode and the HOPG sample working electrode with Karlrez® o-ring. Electrochemical cyclic voltammetry and chronoamperometry experiments were carried out with a potentiostat/galvanostat coupled with the AFM (EC-AFM, Agilent 5500 AFM/SPM). In a typical experiment after the electrochemical treatment the electrode surface was extensively rinsed with dry DMSO and dried under Ar. Images were acquired using an insulating triangular Si tip PointProbe® Plus Non-Contact/Soft Tapping Mode (radius < 10 nm force constant 48 N m^{-1}, resonance frequency 157.85 kHz) in non-contact mode.

3. Results and discussions

Fig. 1a shows a typical cyclic voltammogram of HOPG in an oxygen saturated 0.1 M $LiPF_6$ in DMSO solution. The starting potential and

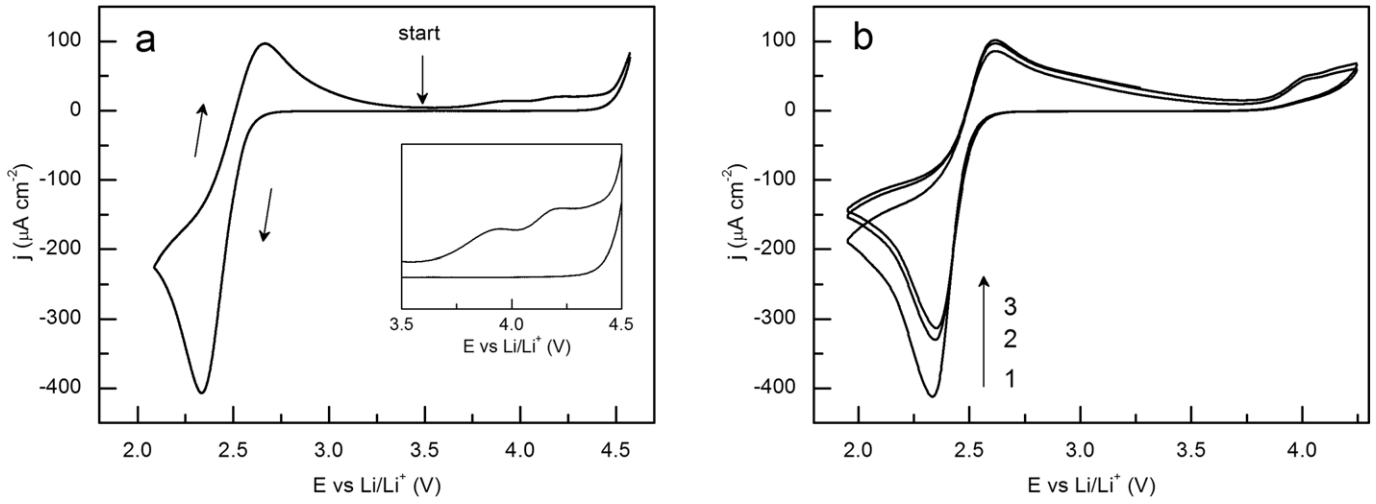

Fig. 1. (a) Cyclic voltammetry of HOPG in 0.1 M $LiPF_6$ in DMSO at 0.1 V s^{-1}. The starting potential and sweep direction is indicated. Inset magnifies the CV in the 3.5–4.5 V range. (b) Consecutive CVs of HOPG in 0.1 M $LiPF_6$ in DMSO at 0.1 V s^{-1}.

sweep direction are shown in the figure. Sweeping the potential in the negative direction results in a clear cathodic peak at 2.3 V which corresponds to the reduction of molecular oxygen on the HOPG surface. The first step of O_2 reduction in aprotic solvents is the formation of the soluble radical anion superoxide O_2^- which, under the strong polarization of O_2^- by Li^+, undergoes disproportionation to insoluble lithium peroxide and molecular oxygen [27]. Reversing the potential sweep results in an anodic peak at 2.6 V which is due to the oxidation of the solvated lithium superoxide adjacent to the electrode. Further excursion in the positive potential (3.75–4.5 V) shows other anodic processes due to the oxidation of the O_2 reduction products and the HOPG surface [28]. Finally above 4.5 V the electrochemical oxidation of the solvent is apparent. Fig. 1b shows three consecutive cyclic voltammograms of HOPG in an oxygen saturated 0.1 M $LiPF_6$ in DMSO solution. Clearly the total anodic and cathodic current densities decrease with cycle number suggesting the cumulative deposition of unreactive surface species.

In order to determine the morphology and chemical nature of the surface species formed after the redox reactions, ex-situ AFM, XPS and UPS measurements we carried out before and after chronoamperometric transients. Thus a potential step from the open circuit potential to 2.05 V (reduction) or to 4.5 V (oxidation) was applied. The duration of both the cathodic and anodic polarization was 180 s and the charge involved was −4.5 mC for the reduction step and 22.5 mC for the oxidation step. Note that the anodic charge is much larger than the cathodic charge as in parallel to the oxidation of surface deposits there is decomposition of the solvent taking place.

Fig. 2 shows AFM images corresponding to: (a) the clean HOPG substrate, (b) HOPG after cathodic treatment at 2.05 V and (c) HOPG after anodic treatment at 4.5 V. Fig. 2a shows the clean HOPG surface with well-defined, wide and atomically flat terraces separated by clearly defined step edges. Fig. 2b shows that applying a cathodic potential of 2.05 V resulted in drastic changes. Indeed, surface deposits of the

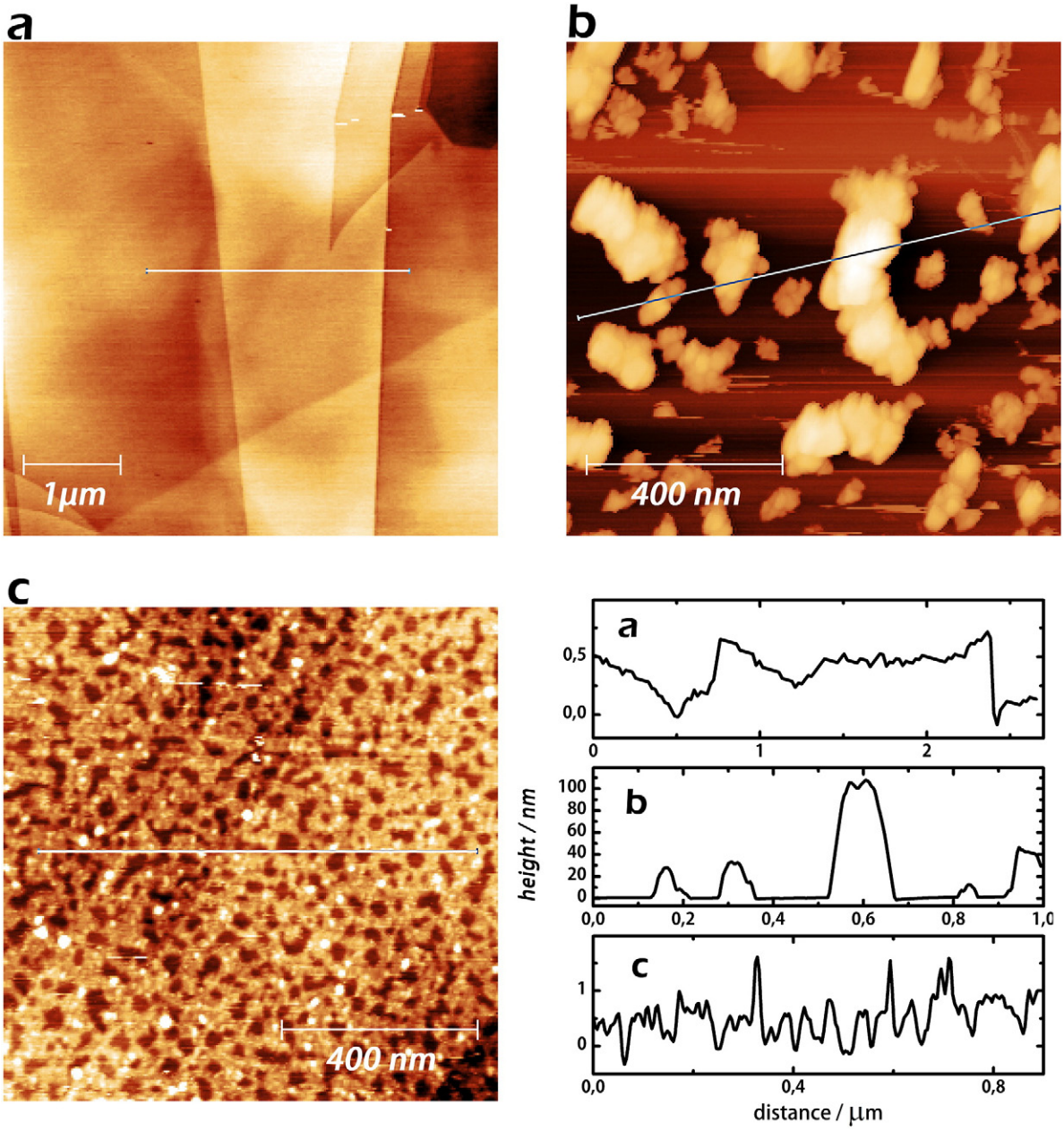

Fig. 2. AFM images of HOPG (a) before electrochemical treatment, (b) after cathodic treatment at 2.05 V and (c) after anodic treatment at 4.5 V. Line profiles are also shown.

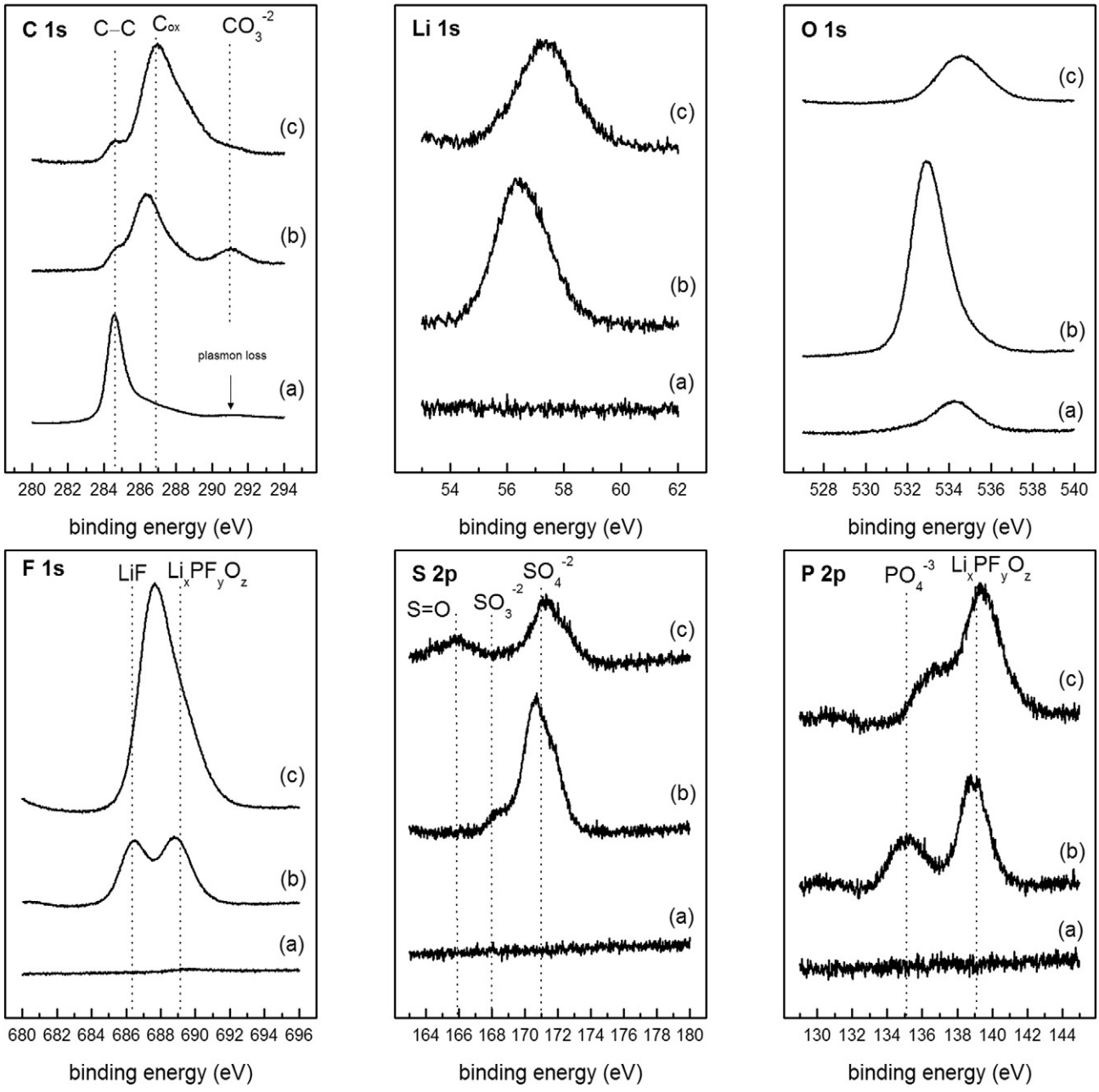

Fig. 3. XPS core level emission spectra of HOPG (a) before electrochemical treatment, (b) after cathodic treatment at 2.05 V and (c) after anodic treatment at 4.5 V.

oxygen reduction products can be observed in an otherwise uncovered HOPG surface. The corresponding line profile indicates that the height of the deposits varies from 20 to 100 nm. It is important to observe that a considerable fraction of the substrate surface remains free of large deposits where oxidation of superoxide anions could take place, unlike the behavior of Au surfaces which completely passivate under these conditions [25]. Note that the amount of the deposit is a function of the polarization time and its nature (large particles versus thin films) depends on the nature of the solvent and the current density employed. Finally, Fig. 2c shows that applying an anodic potential of 4.5 V did not restore the initial condition. In this case, oxidation of the oxygen reduction products resulted in a very thin deposit (approx. 1 nm) that spreads all over the substrate.

The chemical nature of the surface deposits observed by AFM was determined by XPS measurements. Spectra for the C 1s, Li 1s, O 1s, F 1s, S 2p and P 2p XP core level emission lines corresponding to the HOPG surface (a) before electrochemical treatment, (b) after cathodic treatment at 2.05 V and (c) after anodic treatment at 4.5 V are shown in Fig. 3. The bottom spectrum corresponds to the clean HOPG surface. The only elements present on the initial HOPG surface are C and O, all other regions appear flat. Indeed, the C 1s XP spectrum shows a main peak centered at 284.7 eV which is characteristic of HOPG and represents C—C bonds. There is also a little contribution at higher binding energy due to oxidized carbon probably at step edges and defects and plasmon loss features above 291.5 eV.

Cathodic treatment at 2.05 V results in the attenuation of the HOPG related signals due to the surface deposits formed. In the ideal scenario

Table 1
Li Normalized elemental composition excluding C.

	Li	F	O	S	P
2.05 V	100	43	62	5	5
4.5 V	100	88	20	4	7

Table 2
Li containing compounds in percentage.

	Li_2O_2	LiF	Others
2.05 V	42	28	30
4.5 V	0	78	22

the only surface deposit should be Li_2O_2 which is formed after disproportionation of the superoxide anion followed by precipitation over the electrode as discussed above. Indeed, XPS reveals the presence of Li and a large increase in the O 1s signal. However, there are also large F 1s, S 2p and P 2p signals which reveal the presence of unexpected species. The F 1s signal consists of at least two components which can be attributed to LiF at 686.2 eV [23] and $Li_xPF_yO_z$ at 688.9 eV [23]. These signals provide strong evidence that under reduction potentials there is decomposition of the electrolyte ($LiPF_6$) over the HOPG surface as this could be the only source of F^- anions. The S 2p signal has two main contribution, one at 170.6 eV due to SO_4^{2-} [24] and the other one at 168.1 eV due to SO_3^{2-} [24]. Hence, decomposition of the dimethyl sulfoxide solvent is also taking place under cathodic polarization, in agreement with previous observations [24]. Here we should note that electrolyte decomposition is taking place at the interface with the Li_2O_2 particles formed over the HOPG surface given that it is well established that $LiPF_6$ decomposes to form LiF together with P—O bond containing compounds when exposed to Li_2O_2 [21]. The P 2p signals which show the presence of PO_4^{3-} (135.1 eV) and $Li_xPF_yO_z$ (139 eV) give further evidence for electrolyte decomposition. Whereas the C 1s signals with main contributions at 286 eV (C—O containing compounds) and 291 eV (Li_2CO_3) give further evidence for solvent decomposition. The signal at 284.7 eV due to the C—C in HOPG decreased in intensity but can still be observed as there are large areas of the substrate which remain uncovered after cathodic treatment as the relevant AFM images show.

The XPS spectra show that the anodic treatment at 4.5 V did not restore the initial condition, indeed Li, F, O, S and P compounds remain present over the HOPG electrode. The first thing to notice is that the O 1s signal decreases significantly with respect to the O 1s signal corresponding to the reduction treatment, indicating the expected oxidation and removal of Li_2O_2 from the HOPG surface. Furthermore, there is a large increase in the F 1s signal whereas the Li 1s signal remains approximately constant. These observations indicate that decomposition of the electrolyte into LiF continues as the Li_2O_2 is removed. This is in line with the increased P 2p signal which also indicates electrolyte decomposition. Note that the Li 1s signal is shifted 0.8 eV towards higher binding energy with respect to the Li signal corresponding to the reduction treatment. This is consistent with the increase coverage of LiF and simultaneous decrease of Li_2O_2 and Li_2CO_3. The decrease of lithium carbonate is confirmed by the decrease in the 290.2 eV contribution in the C1s region. The C 1s spectrum corresponding to the anodic treatment also shows an increase in the C—O containing compounds indicating further decomposition of the solvent under oxidative potentials in line with the S 2p signal. Here we should point out that the attenuation of the C 1s contribution at 284.7 eV corresponding to C—C in HOPG after anodic treatment is much smaller than the expected attenuation for an overlayer of approximately 1 nm thickness as observed by AFM. This implies that anodic treatment partly oxidizes the topmost layer of the HOPG substrate. This is consistent with the increase in the 287 eV contribution of the C 1s signal and with the observations of Wen et al. who reported that HOPG substrates are oxidized in the 4.2–4.4 V overpotential range [28].

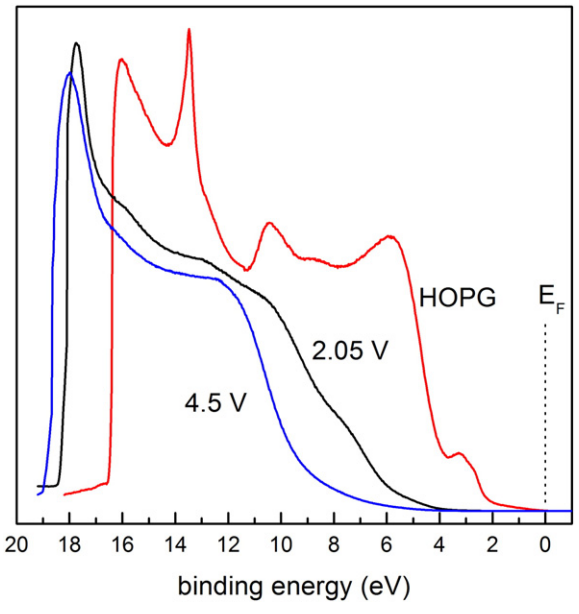

Fig. 4. UPS spectra of HOPG before electrochemical treatment (red), after cathodic treatment at 2.05 V (black) and after anodic treatment at 4.5 V (blue).

The surface elemental composition could be estimated from the core levels XPS integrated intensities after instrumental and photoionization cross section corrections. This is shown in Table 1 normalized with respect to the Li signal and excluding the C signal to exclude the HOPG contributions.

Here we should bear in mind that the analysis depth of XPS is approximately 6 nm (3 times the photoelectron attenuation length). As shown in the AFM images above, in the cathodic treatment (2.05 V) surface deposits have heights in the 20–100 nm range, therefore XPS is only probing the topmost layer of the deposit excluding its core from the analysis. On the other hand, deposits formed after the anodic treatment constitute a thin film of approximately 1 nm thickness, thus observed in full by XPS. Clearly Li, F and O are the dominant surface elements (around 95%) whereas S and P are in smaller quantities (around 5%). As discussed above going from 2.05 V to 4.5 V results in a large increase in the F surface amount accompanied by a large decrease in the O surface amount due to the Li_2O_2 oxidation. This could be seen easily in Table 2 which shows the percentage of Li containing surface compounds. After reductive potentials the top approximately 6 nm of the 20–100 nm surface deposits are composed of mainly Li_2O_2 (42%), LiF (28%) and the sum of Li_2CO_3, Li_2SO_4 and Li_3PO_4 (30%). Whereas oxidative potentials result in a 1 nm thin film of mainly LiF (78%) deposited over the HOPG electrode.

Fig. 4 shows the UPS spectra of the HOPG electrode before electrochemical treatment (red), after cathodic treatment at 2.05 V (black) and after anodic treatment at 4.5 V (blue). Spectrum corresponding to the clean HOPG substrate shows the characteristic valence band structure with bands between 0 and 9 eV. The sharp emission at 13.6 eV is characteristic of electrons that are inelastically scattered into a high density of states region of the HOPG conduction bands [29]. From the high binding energy cut-off a work function of 4.8 eV could be determined for the initial HOPG surface in agreement with literature values [30]. Cathodic treatment results in a large attenuation of the substrate band structure and a decrease of the sample work function to 3.2 eV. This value is consistent with the measured work function of Li_2CO_3 deposited over graphene layers [31]. Anodic treatment at 4.5 V results in further attenuation of the substrate surface bands consistent with a deposit that covers most of the HOPG surface and a work function of 2.5 eV. This low work function value is due to the dielectric thin LiF film deposited over the HOPG substrate [32] and is in complete agreement with the experiments of Schlaf and co-workers who reported 2.5 eV for the work function of 3 nm thick LiF films grown on Al substrates [33].

4. Conclusions

A systematic and thorough surface study of the O_2/Li_2O_2 electrode reaction over HOPG electrodes in 0.1 M $LiPF_6$ in DMSO was carried out. AFM, XPS and UPS measurements indicate that operation under cathodic potentials resulted in the deposition of large particles (20–100 nm in height) composed mainly of Li_2O_2, LiF, Li_2CO_3 and other species related to the decomposition of both the $LiPF_6$ electrolyte and DMSO solvent. Furthermore, applying anodic potentials resulted in the deposition of an approximately 1 nm in thickness thin film of mainly LiF which causes a large work function decrease of the substrate. The results presented here demonstrate the high reactivity of the oxygen reduction products towards the electrolyte and solvent forming deposits which remain on the surface even after high anodic potentials. These findings help to rationalize the observed loss of capacity in Li–air batteries.

Acknowledgments

Funding from CONICET and ANPCyT PICT 2012 1452 and FS-Nano 07 is gratefully acknowledged.

References

[1] P.G. Bruce, S.A. Freunberger, L.J. Hardwick, J.-M. Tarascon, Nat. Mater. 11 (2011) 172.
[2] J. Christensen, P. Albertus, R.S. Sanchez-Carrera, T. Lohmann, B. Kozinsky, R. Liedtke, J. Ahmed, A. Kojic, J. Electrochem. Soc. 159 (2012) R1.
[3] L.J. Hardwick, P.G. Bruce, Curr. Opin. Solid State Mater. Sci. 16 (2012) 178.
[4] C.J. Bondue, A.A. Abd-el-latif, P. Hegemann, H. Baltruschat, J. Electrochem. Soc. 162 (2015) A479.
[5] K.M. Abraham, J. Electrochem. Soc. 143 (1996) 1.
[6] T. Ogasawara, A. Débart, M. Holzapfel, P. Novák, P.G. Bruce, J. Am. Chem. Soc. 128 (2006) 1390.
[7] N.B. Aetukuri, B.D. McCloskey, J.M. García, L.E. Krupp, V. Viswanathan, A.C. Luntz, Nat. Chem. 7 (2014) 50.
[8] L. Johnson, C. Li, Z. Liu, Y. Chen, S.A. Freunberger, P.C. Ashok, B.B. Praveen, K. Dholakia, J.-M. Tarascon, P.G. Bruce, Nat. Chem. 6 (2014) 1091.
[9] B.D. Adams, C. Radtke, R. Black, M.L. Trudeau, K. Zaghib, L.F. Nazar, Energy Environ. Sci. 6 (2013) 1772.
[10] D.G. Kwabi, T.P. Batcho, C.V. Amanchukwu, N. Ortiz-Vitoriano, P. Hammond, C.V. Thompson, Y. Shao-Horn, J. Phys. Chem. Lett. 5 (2014) 2850.
[11] C.O. Laoire, S. Mukerjee, K.M. Abraham, E.J. Plichta, M.A. Hendrickson, J. Phys. Chem. C 114 (2010) 9178.
[12] Z. Peng, S.A. Freunberger, Y. Chen, P.G. Bruce, Science 337 (80-) (2012) 563.
[13] M.J. Trahan, S. Mukerjee, E.J. Plichta, M.A. Hendrickson, K.M. Abraham, J. Electrochem. Soc. 160 (2013) A259.
[14] D. Xu, Z. Wang, J. Xu, L. Zhang, X. Zhang, Chem. Commun. 48 (2012) 6948.
[15] B.D. Mccloskey, A. Valery, A.C. Luntz, S.R. Gowda, G.M. Wallraff, J.M. Garcia, T. Mori, L.E. Krupp, J. Phys. Chem. Lett. 4 (2013) 2989.
[16] B.D. McCloskey, R. Scheffler, A. Speidel, G. Girishkumar, A.C. Luntz, J. Phys. Chem. C 116 (2012) 23897.
[17] B.D. McCloskey, A. Speidel, R. Scheffler, D.C. Miller, V. Viswanathan, J.S. Hummelshøj, J.K. Nørskov, A.C. Luntz, J. Phys. Chem. Lett. 3 (2012) 997.
[18] C.J. Barile, A.A. Gewirth, J. Electrochem. Soc. 160 (2013) A549.
[19] B.D. McCloskey, D.S. Bethune, R.M. Shelby, G. Girishkumar, A.C. Luntz, J. Phys. Chem. Lett. 2 (2011) 1161.
[20] N. Tsiouvaras, S. Meini, I. Buchberger, H.A. Gasteiger, J. Electrochem. Soc. 160 (2013) A471.
[21] R. Younesi, M. Hahlin, F. Björefors, P. Johansson, K. Edström, Chem. Mater. 25 (2013) 77.
[22] R. Younesi, P. Norby, T. Vegge, ECS Electrochem. Lett. 3 (2014) A15.
[23] D. Chalasani, B.L. Lucht, ECS Electrochem. Lett. 1 (2012) A38.
[24] D. Sharon, M. Afri, M. Noked, A. Garsuch, A.A. Frimer, D. Aurbach, J. Phys. Chem. Lett. 4 (2013) 3115.
[25] W.R. Torres, A.Y. Tesio, E.J. Calvo, Electrochem. Commun. 49 (2014) 38.
[26] L.P. Méndez De Leo, E. de la Llave, D. Scherlis, F.J. Williams, J. Chem. Phys. 138 (2013) 114707.
[27] S.E. Herrera, A.Y. Tesio, R. Clarenc, E.J. Calvo, Phys. Chem. Chem. Phys. 16 (2014) 9925.
[28] R. Wen, M. Hong, H.R. Byon, J. Am. Chem. Soc. 135 (2013) 10870.
[29] J. Magulick, M.M. Beerbom, B. Lägel, R. Schlaf, J. Phys. Chem. B 110 (2006) 2692.
[30] S. Suzuki, C. Bower, Y. Watanabe, O. Zhou, Appl. Phys. Lett. 76 (2000) 4007.
[31] K.C. Kwon, K.S. Choi, B.J. Kim, J.L. Lee, S.Y. Kim, J. Phys. Chem. C 116 (2012) 26586.
[32] S. Prada, U. Martinez, G. Pacchioni, Phys. Rev. B 78 (2008).
[33] R. Schlaf, B.A. Parkinson, P.A. Lee, K.W. Nebesny, G. Jabbour, B. Kippelen, N. Peyghambarian, N.R. Armstrong, J. Appl. Phys. 84 (1998) 6729.